nature portfolio

https://doi.org/10.1038/s41586-022-05409-2

Supplementary information

A ligand insertion mechanism for cooperative NH_3 capture in metal–organic frameworks

In the format provided by the authors and unedited

Supplementary Information for

A Ligand Insertion Mechanism for Cooperative NH_3 Capture in Metal–Organic Frameworks

Benjamin E. R. Snyder, Ari B. Turkiewicz, Hiroyasu Furukawa, Maria V. Paley, Ever O. Velasquez, Matthew N. Dods, Jeffrey R. Long*

Correspondence to: jrlong@berkeley.edu

This PDF file includes:

Supplementary Figures 1 to 37
Supplementary Tables 1 to 4

Table of Contents

1. Preliminary characterization of Cu(cyhdc)

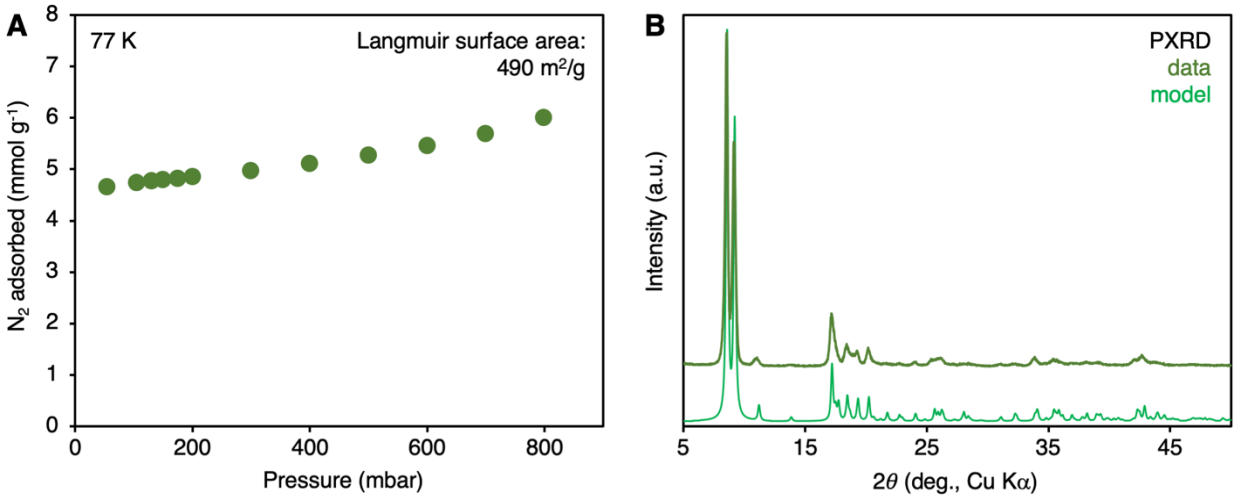

Supplementary Figure 1. (**A**) Nitrogen adsorption isotherm obtained for Cu(cyhdc) at 77 K. The data were used to calculate a Langmuir surface area of 490 m^2/g. (**B**) The powder x-ray diffraction pattern obtained for microcrystalline Cu(cyhdc) (yellow green) compared with the powder x-ray diffraction pattern simulated from the crystal structure of Cu(cyhdc) reported in reference 18 in the main text.

2. High pressure NH_3 isotherms of Cu(cyhdc) at 298 and 373 K

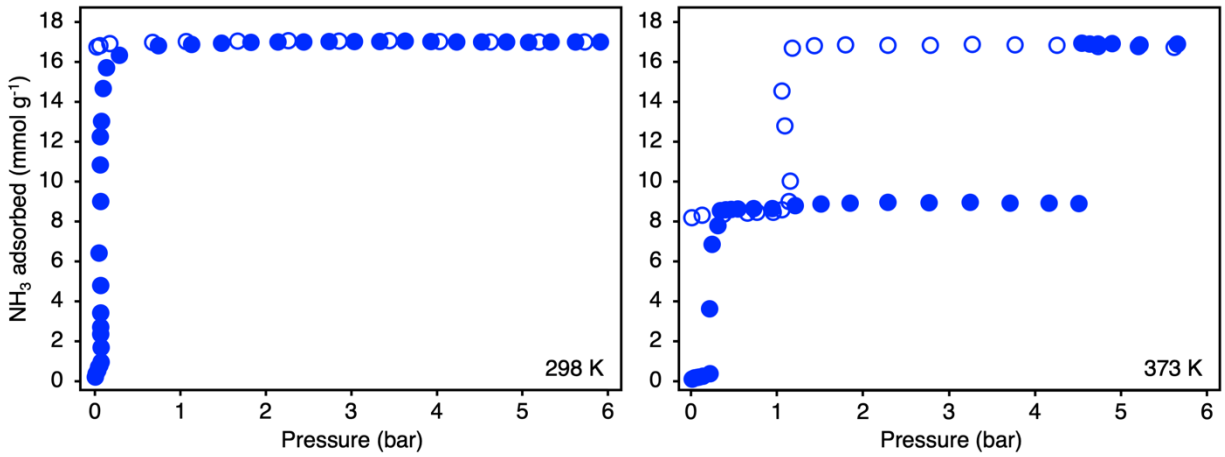

Supplementary Figure 2. High pressure NH_3 adsorption (filled circles) and desorption (empty circles) isotherms collected for Cu(cyhdc) at 298 K (left) and 373 K (right). At 373 K, the onset pressure for the second adsorption step could not be reliably determined, as it proved difficult to capture data points in the middle of this step due to the constant-pressure dosing mode of the gas adsorption analyzer used for these measurements. We can estimate from the data that the step onset pressure lies around 4.5 bar at this temperature.

3. Powder x-ray diffraction analysis of NH_3-dosed Cu(cyhdc)

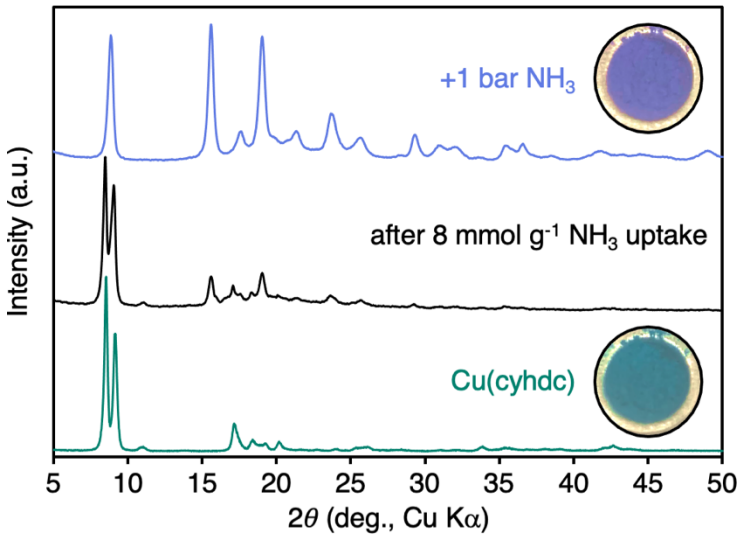

Supplementary Figure 3. Comparison of powder x-ray diffraction patterns for pristine Cu(cyhdc) (green trace) and for the sample after partial and complete loading with NH_3 at 298 K (black and blue traces, respectively). The data indicate that, at this temperature, NH_3 adsorption involves a direct transition from Cu(cyhdc) to $Cu(NH_3)_4$(cyhdc), with no intermediate phase observed. Images showing the color of the material before and after NH_3 dosing are included above the corresponding powder x-ray diffraction data.

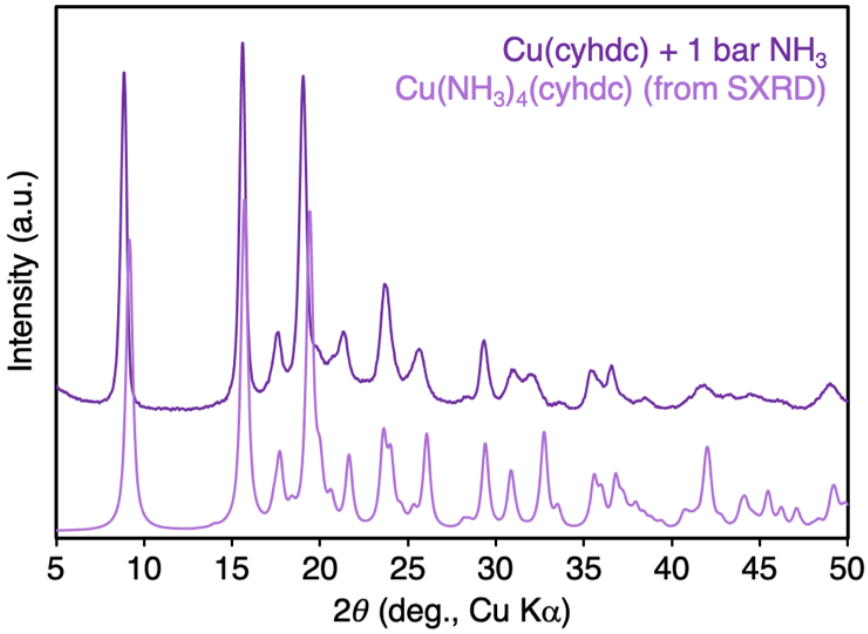

Supplementary Figure 4. Comparison of the powder x-ray diffraction pattern for Cu(cyhdc) following exposure to 1 atm NH_3 at 298 K (dark purple) with the powder x-ray diffraction pattern predicted from the single-crystal x-ray diffraction structure of $Cu(NH_3)_4$(cyhdc).

4. Analysis of NH_3 desorption from $Cu(NH_3)_4(cyhdc)$ and NH_3 adsorption by Cu(bdc)

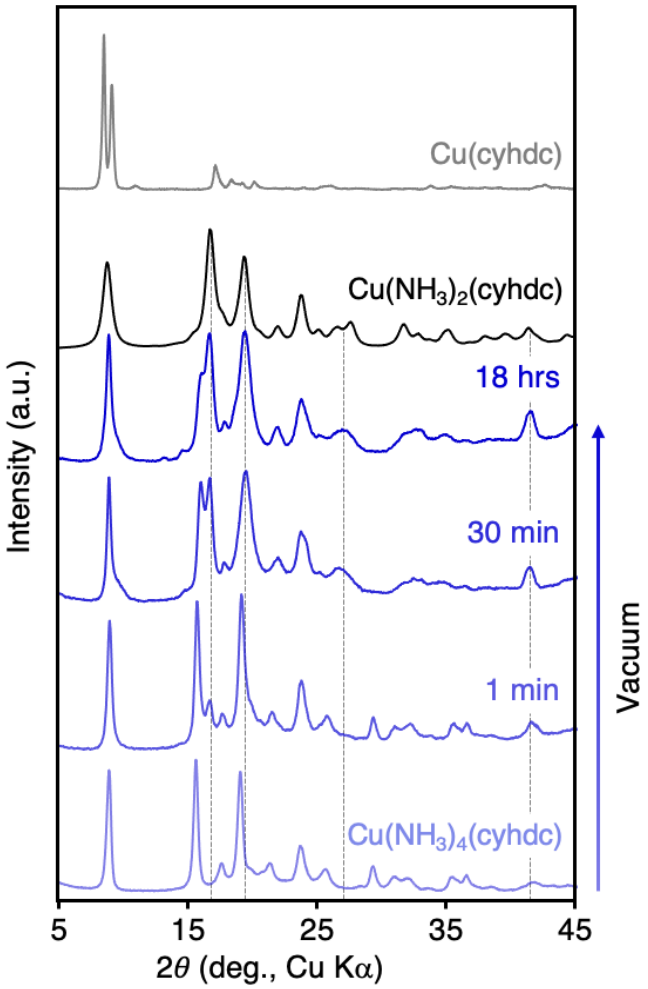

Supplementary Figure 5. Powder x-ray diffraction patterns collected at various time intervals while pulling vacuum on a sample of pristine $Cu(NH_3)_4(cyhdc)$ (bottom trace). The diffraction pattern collected after 18 hours closely matches that predicted based on the single-crystal x-ray diffraction structure of $Cu(NH_3)_2(cyhdc)$ (black trace), indicating that the conversion to $Cu(NH_3)_2(cyhdc)$ is essentially complete.

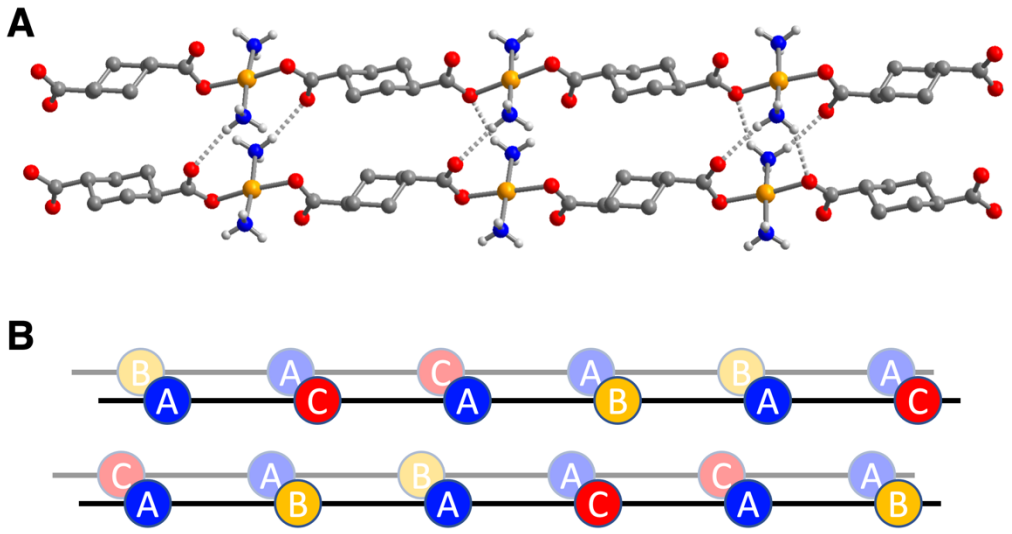

Supplementary Figure 6. (**A**) Portion of the structure of $Cu(NH_3)_2(cyhdc)$ obtained from single crystal x-ray diffraction analysis, showing hydrogen bonding interactions between two neighboring chains. (**B**) Illustration of long range order in the crystal structure of $Cu(NH_3)_2(cyhdc)$. The crystal structure contains three symmetrically distinct copper(II) ions, Cu_A (blue), Cu_B (gold), and Cu_C (red). Cu_B and Cu_C lie on inversion centers. There are therefore three symmetrically distinct linkers, defined by the species of Cu they bridge (Cu_A-Cu_B/Cu_B-Cu_A, Cu_A-Cu_C/Cu_C-Cu_A, and Cu_B-Cu_C/Cu_C-Cu_B). Within a given chain, the ordering of copper(II) ions is Cu_A-Cu_B-Cu_A-Cu_C-. Chains are offset with respect to their neighbors, as illustrated. See the corresponding cif file for full structural details.

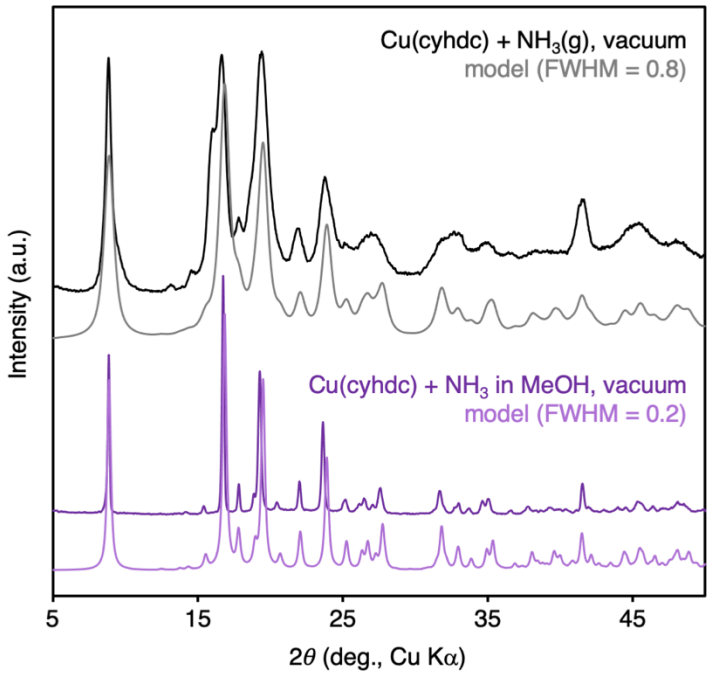

Supplementary Figure 7. (Top) Powder x-ray diffraction pattern collected for a sample of Cu(cyhdc) after dosing with 1 bar of NH_3 and subsequent evacuation for 18 hours under dynamic vacuum at room temperature (black trace). The pattern simulated from the crystal structure of $Cu(NH_3)_2$(cyhdc) is shown for comparison (gray trace, peak full width at half maximum = 0.8 2θ). (Bottom) Powder x-ray diffraction pattern obtained from a sample of $Cu(NH_3)_2$(cyhdc) prepared as described in the Methods section and evacuated for 18 hours at room temperature under dynamic vacuum (dark purple trace). The pattern simulated from the crystal structure of $Cu(NH_3)_2$(cyhdc) is shown for comparison (light purple trace, peak full width at half maximum = 0.2 2θ).

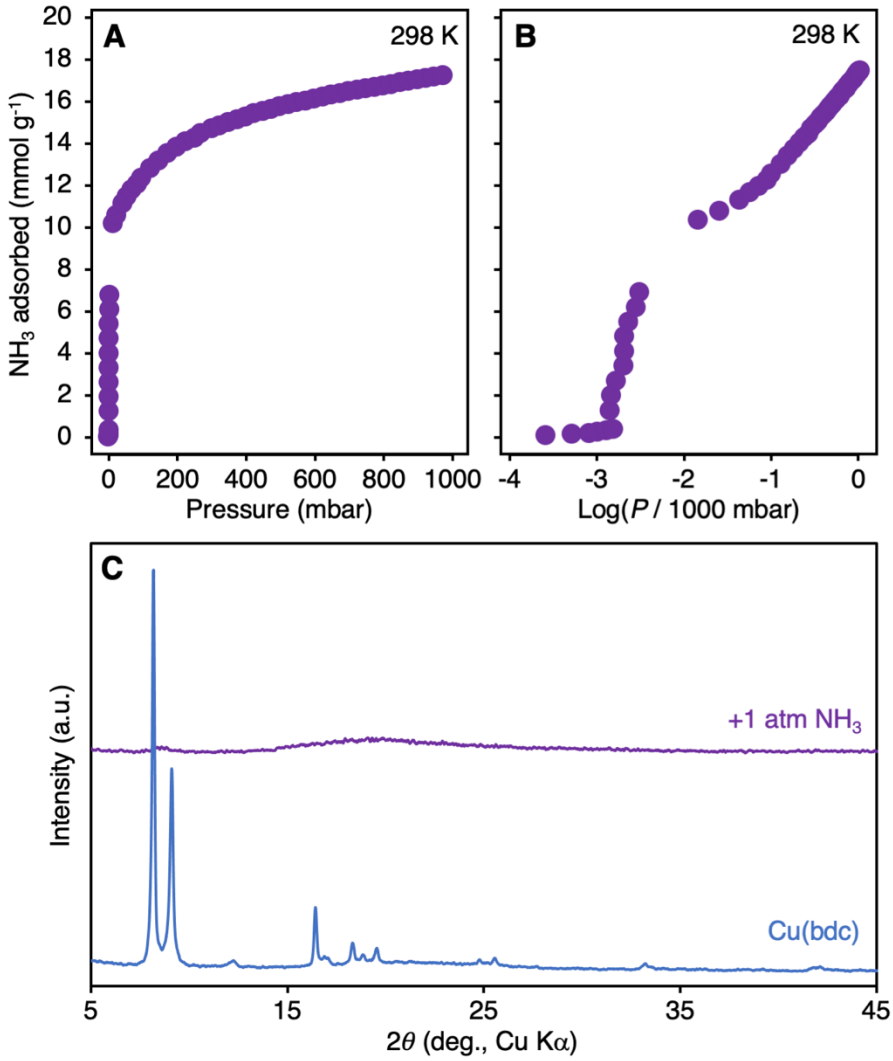

Supplementary Figure 8. (**A**) NH_3 adsorption isotherm for Cu(bdc) collected at 298 K. (**B**) Adsorption data presented in **A** plotted on a logarithmic scale, showing stepped adsorption with a step onset pressure of approximately 1.5 mbar. (**C**) Comparison of powder x-ray diffraction patterns collected for activated Cu(bdc) before (blue trace) and after (purple trace) dosing with 1 atm NH_3 at 298 K, showing loss of crystallinity following NH_3 adsorption.

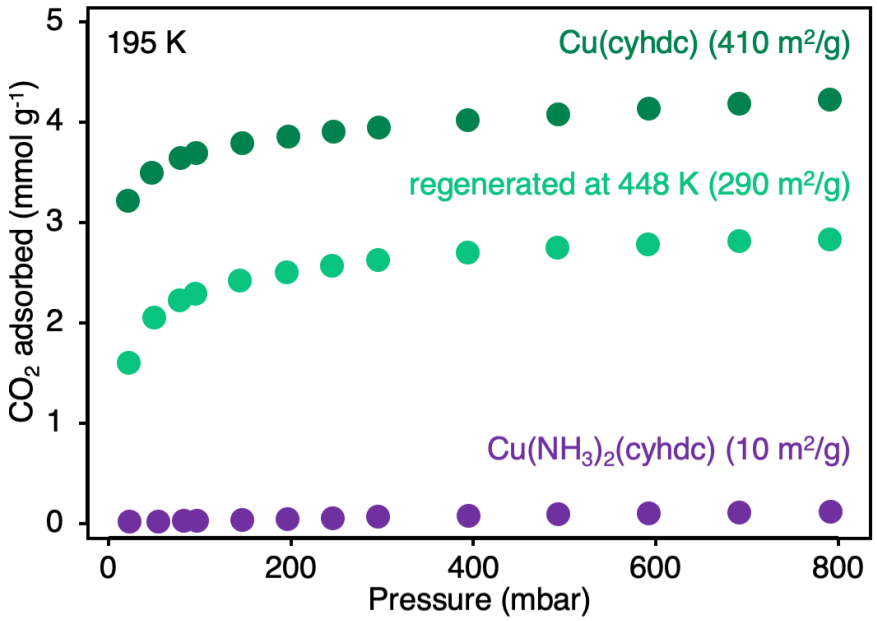

Supplementary Figure 9. CO_2 isotherms obtained at 195 K for pristine Cu(cyhdc) (dark green circles) and a sample of Cu(cyhdc) following regeneration from $Cu(NH_3)_2$(cyhdc) with gradual heating, see Fig. 3a in the main text (light green circles). Langmuir surface areas calculated from these isotherms demonstrate the recovery of microporosity upon regeneration of Cu(cyhdc) from $Cu(NH_3)_2$(cyhdc). The CO_2 isotherm of $Cu(NH_3)_2$(cyhdc) is shown in purple circles for comparison. The lower surface area of the regenerated material may be due to structural imperfections that block its one-dimensional pores. As a result, the material does not express microporosity at 77 K.

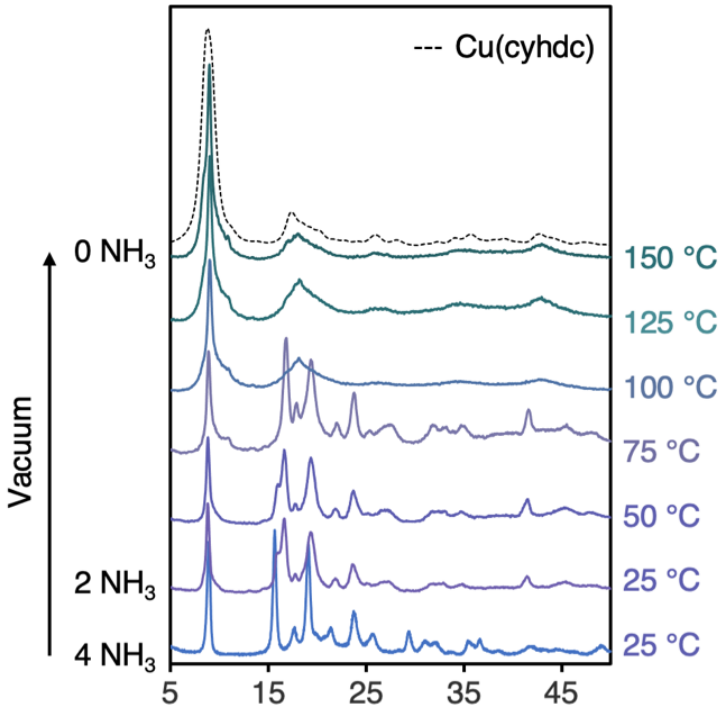

Supplementary Figure 10. Powder x-ray diffraction data tracking the conversion of $Cu(NH_3)_4$(cyhdc) (bottom blue trace) to Cu(cyhdc) (top green trace) with heating under dynamic vacuum. The starting sample of $Cu(NH_3)_4$(cyhdc) was prepared by dosing Cu(cyhdc) with 1 bar NH_3 at 298 K. Samples were held at the indicated temperatures for 24 hours. The powder x-ray diffraction pattern for pristine Cu(cyhdc) (generated from the single-crystal structure of Cu(cyhdc) with a full-width half-max of 1.2º 2θ) is shown for comparison. While peak broadening is observed upon desorption of ammonia, re-dosing the regenerated framework with gaseous NH_3 results in peak narrowing (see Supplementary Fig. 13).

5. Thermogravimetric analysis ammonia desorption from $Cu(NH_3)_4$(cyhdc)

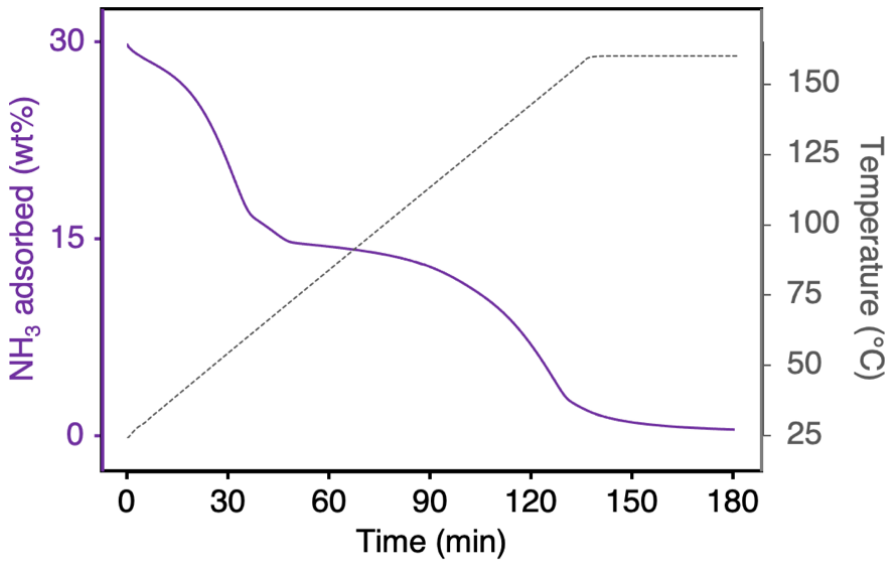

Supplementary Figure 11. Thermogravimetric analysis of NH_3 desorption from $Cu(NH_3)_4$(cyhdc). The data show two mass losses—one from 25 to 50 °C, and another from 100 to 150 °C—each corresponding to loss of two equivalents of NH_3 per copper center.

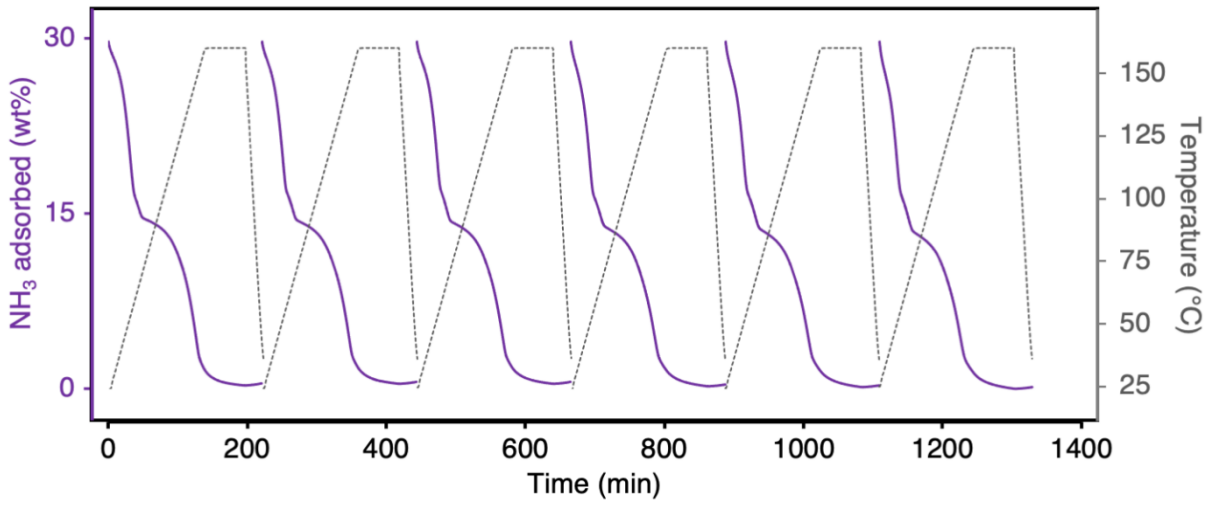

Supplementary Figure 12. Thermogravimetric analysis of NH_3 desorption from $Cu(NH_3)_4$(cyhdc) (see Methods) over the course of six cycles. For each cycle, the material was heated from 25 to 160 °C (ramp rate of 1 °C/min), held for 60 minutes at 160 °C, and then cooled to 25 °C. The sample was subsequently dosed with 1 bar ammonia at 25 °C and held for 30 minutes before another desorption cycle.

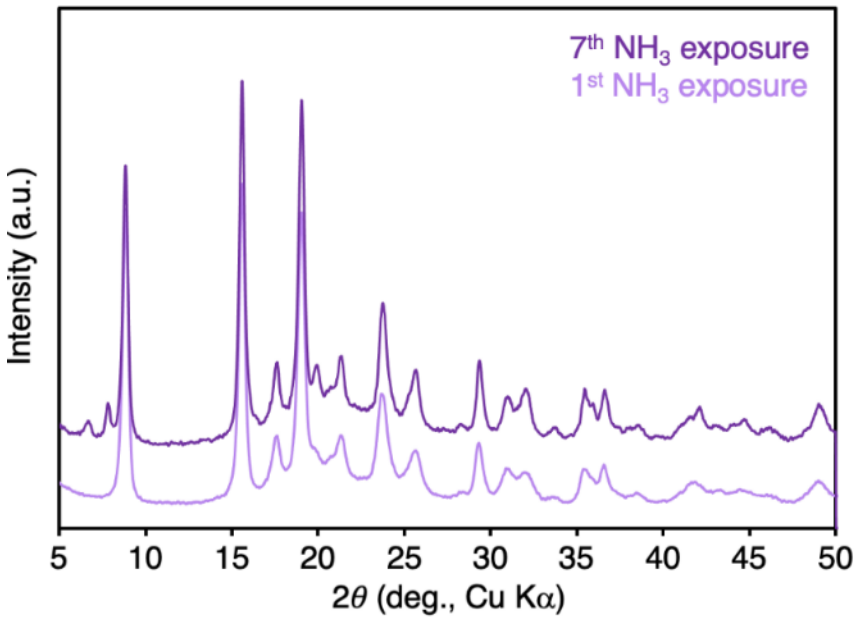

Supplementary Figure 13. Comparison of powder x-ray diffraction patterns collected for $Cu(NH_3)_4(cyhdc)$ formed after initial exposure of Cu(cyhdc) to 1 bar NH_3 (light purple trace) and $Cu(NH_3)_4(cyhdc)$ after repeated ammonia adsorption and desorption cycling (dark purple trace). See Supplementary Fig. 12 and the Methods section.

6. Conceptual illustration of Cu(cyhdc) structure assembled from *cis* Cu(cyhdc) chains

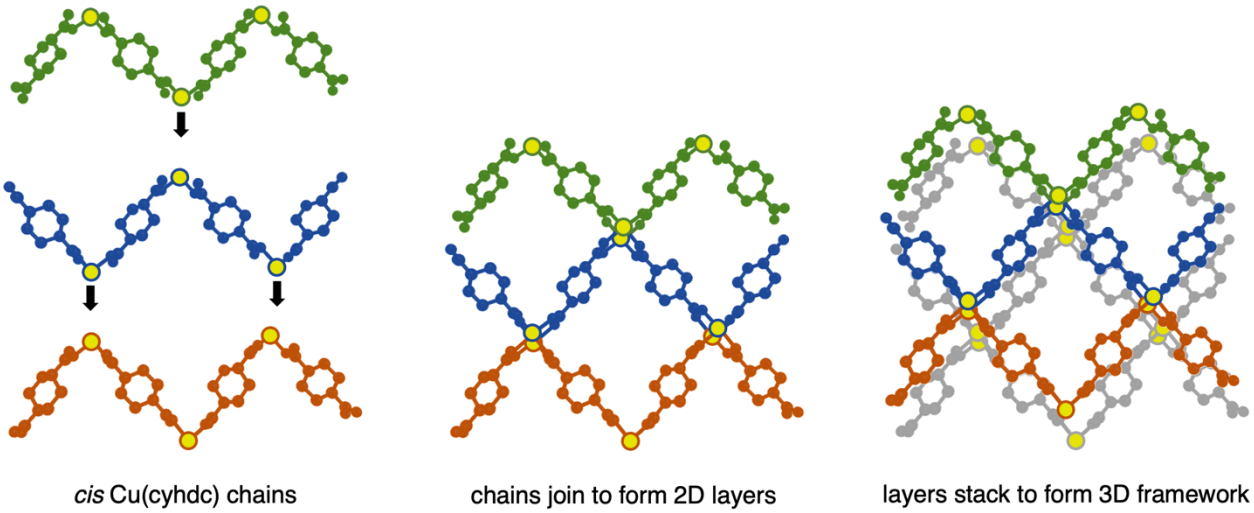

Supplementary Figure 14. Illustration of how *cis* Cu(cyhdc) chains could interact to form the Cu(cyhdc) framework.

7. Fits of ammonia isothermal adsorption data

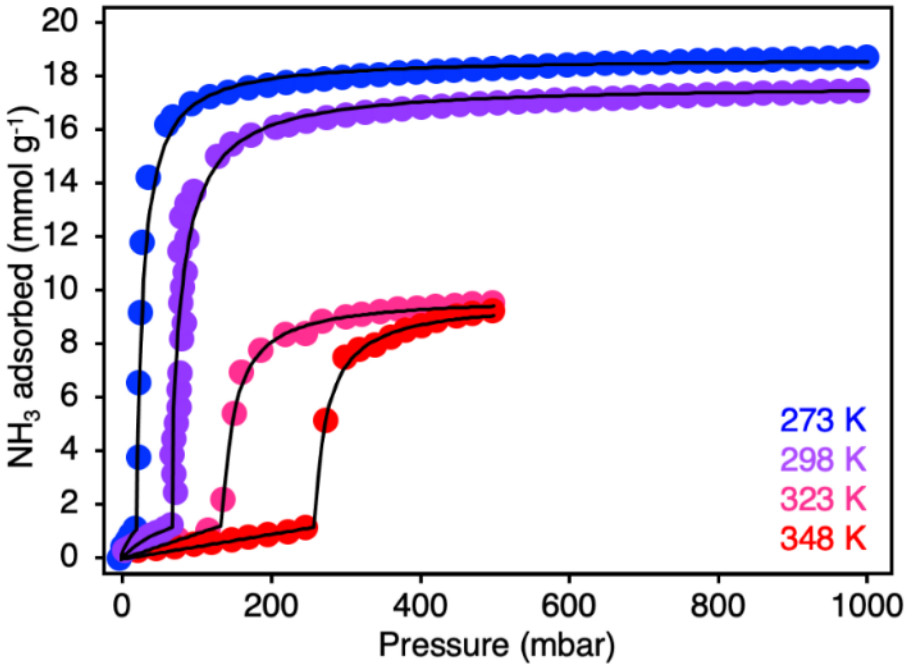

Supplementary Figure 15. Piecewise fits of NH_3 adsorption isotherms of Cu(cyhdc) generated using the method described in reference 22. These fits were used to calculate the isosteric heats of ammonia adsorption presented in Fig. 4b in the main text.

8. High-pressure, high-temperature NH_3, N_2, H_2 adsorption isotherms for Cu(cyhdc)

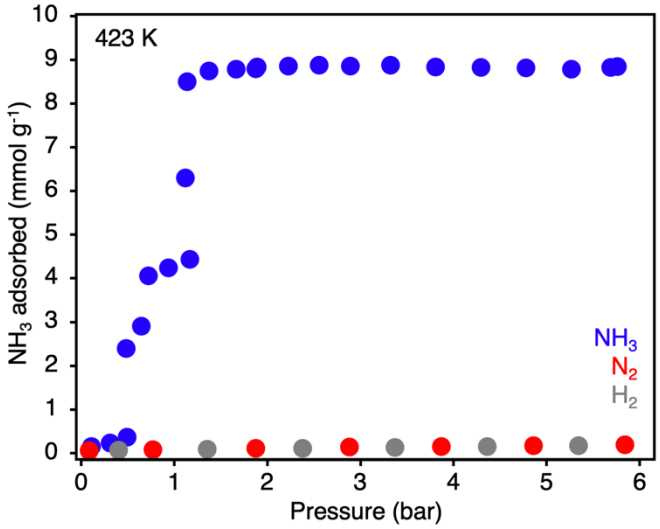

Supplementary Figure 16. Ammonia (blue data), N_2 (red data), and H_2 (gray data) adsorption isotherms collected for Cu(cyhdc) at 423 K, revealing negligible uptake of N_2 and H_2 (< 0.12 mmol/g) under these conditions.

9. Characterization of M(cyhdc) (M = Cr, Fe, Cu) and Cu(dicarboxylate) frameworks

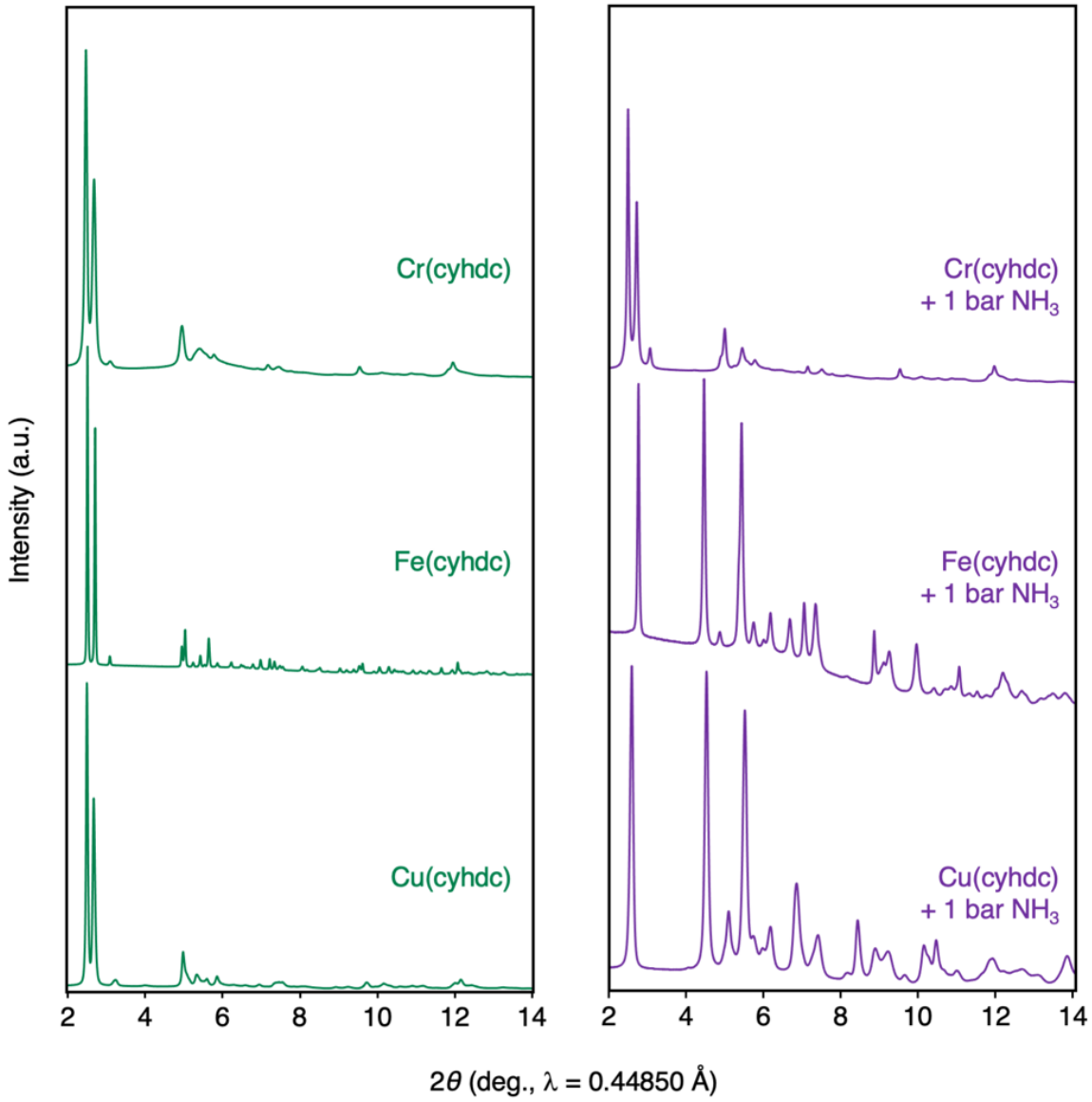

Supplementary Figure 17. (Left) Synchrotron powder x-ray diffraction data collected for microcrystalline samples of activated Cr(cyhdc) (top), Fe(cyhdc) (middle), and Cu(cyhdc) (bottom). (Right) Synchrotron powder x-ray diffraction data collected for microcrystalline samples of Cr(cyhdc) (top), Fe(cyhdc) (middle), and Cu(cyhdc) (bottom) following dosing with 1 bar of NH_3 at room temperature as described in the Methods section; $\lambda = 0.44850$ Å.

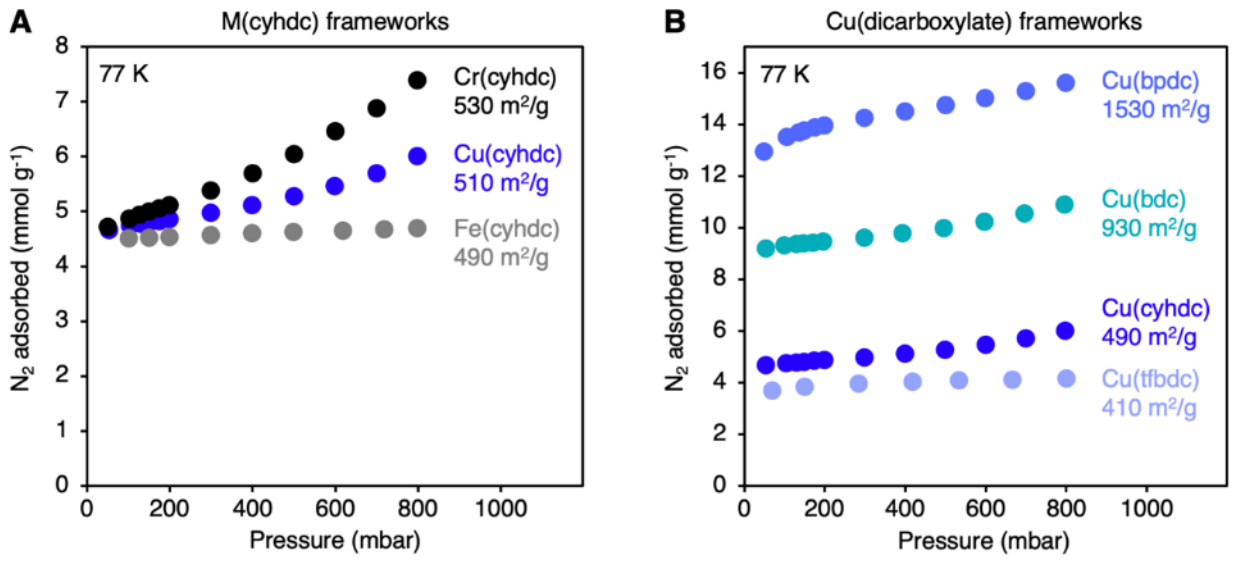

Supplementary Figure 18. Nitrogen adsorption isotherms obtained at 77 K for M(cyhdc) (M = Fe, Cu, Cr) (**A**) and Cu(dicarboxylate) frameworks (dicarboxylate = $bpdc^{2-}$, bdc^{2-}, $cyhdc^{2-}$, $tfbdc^{2-}$) (**B**) and calculated Langmuir surface areas.

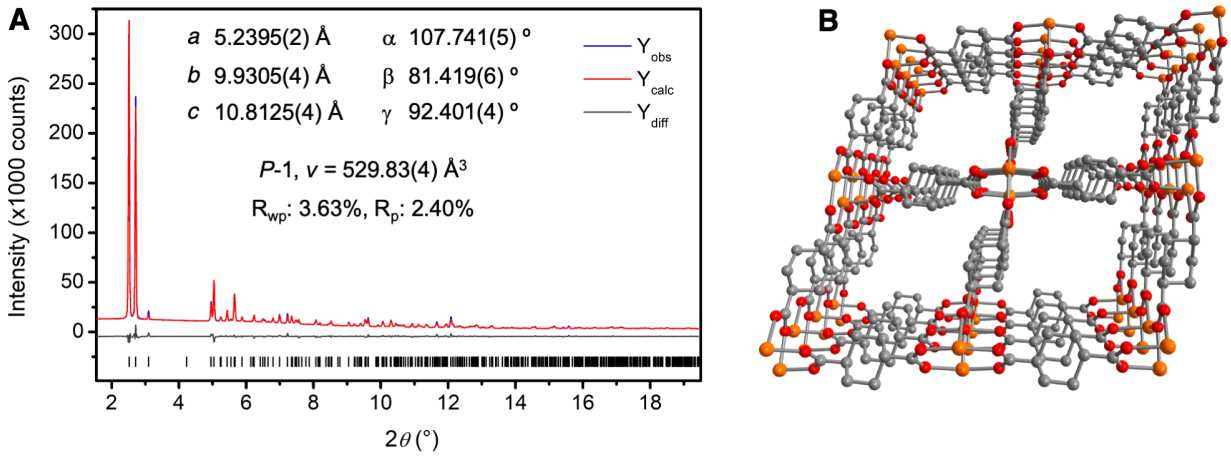

Supplementary Figure 19. (**A**) Rietveld refinement of synchrotron powder x-ray diffraction data collected for Fe(cyhdc) at 298 K (λ = 0.44850 Å). (**B**) Structural model of Fe(cyhdc) derived from the Rietveld refinement. Orange, red, and gray spheres represent Fe, O, and C atoms, respectively; H atoms have been omitted for clarity.

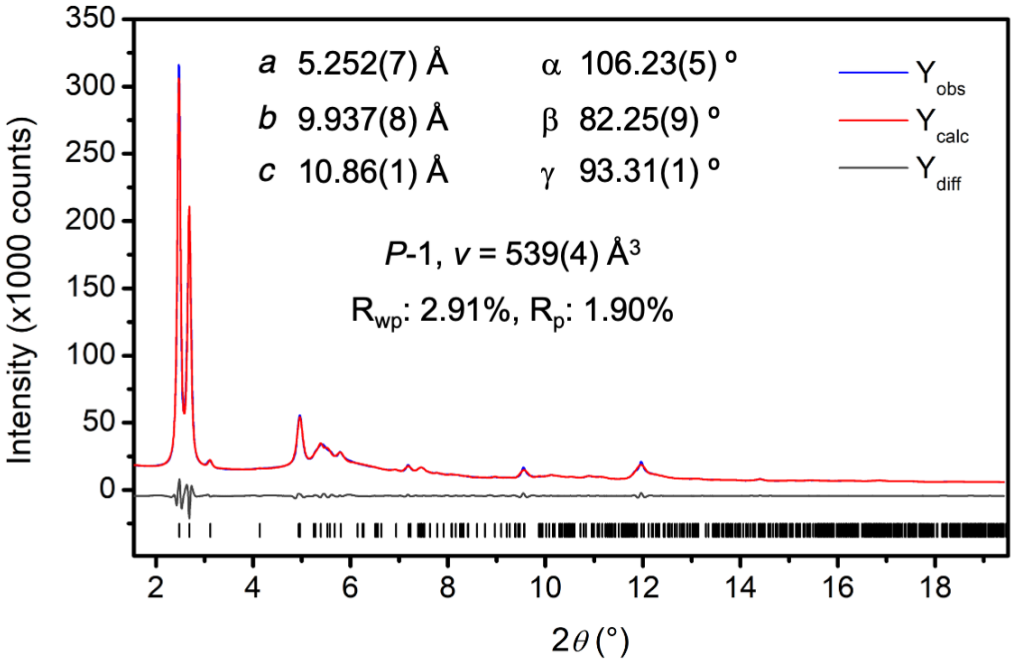

Supplementary Figure 20. Pawley refinement of the unit cell of Cr(cyhdc) from powder x-ray diffraction data collected at 298 K (λ = 0.44850 Å).

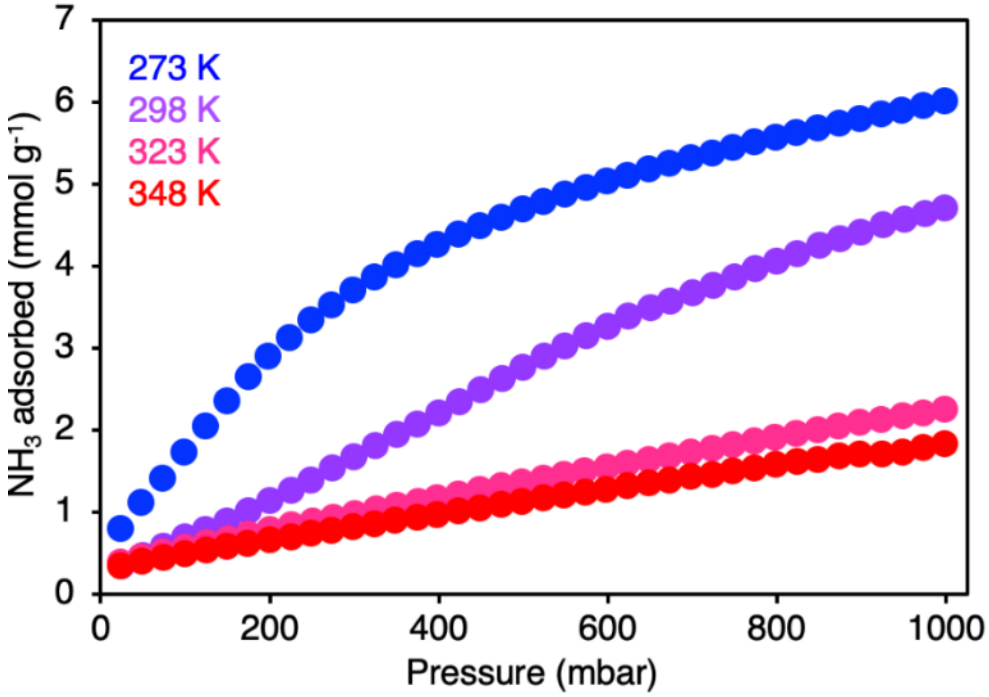

Supplementary Figure 21. Ammonia adsorption isotherms collected for activated, microcrystalline Cr(cyhdc) at the indicated temperatures.

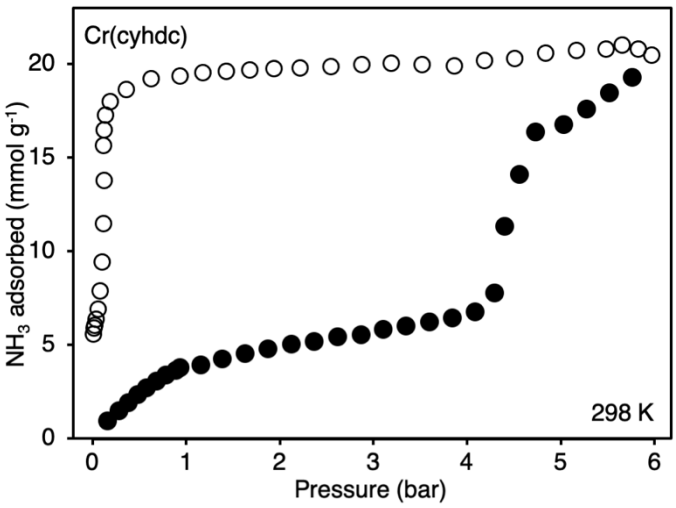

Supplementary Figure 22. High pressure NH_3 adsorption (filled circles) and desorption (empty) circles) data collected from Cr(cyhdc) at 298 K.

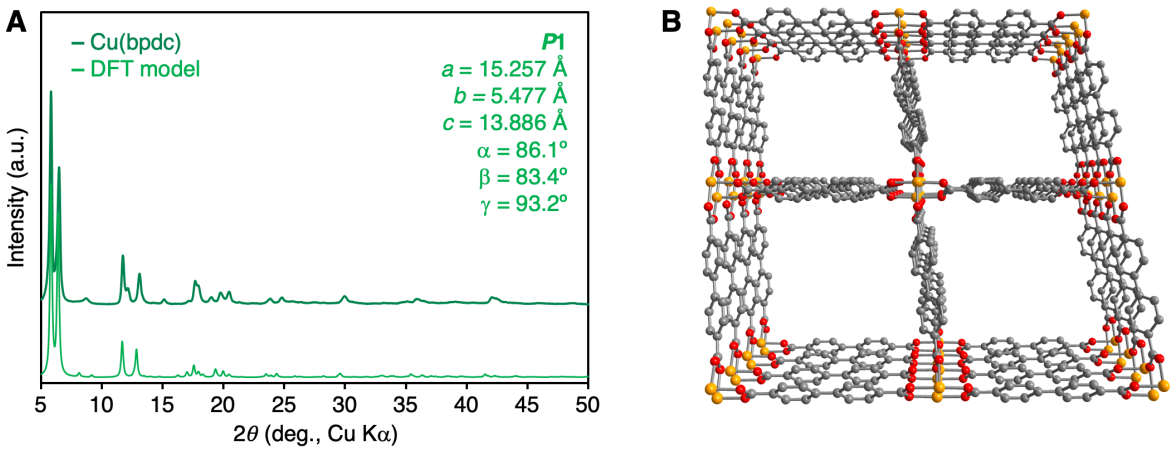

Supplementary Figure 23. (**A**) Powder x-ray diffraction pattern of activated Cu(bpdc) (dark green), compared to the predicted powder pattern for the structural model obtained from DFT calculations (light green). (**B**) DFT structural model of Cu(bpdc). Orange, red, and gray spheres represent Cu, O, and C atoms, respectively; H atoms have been omitted for clarity. Coordinates for this DFT model are reported in Supplementary Table 3.

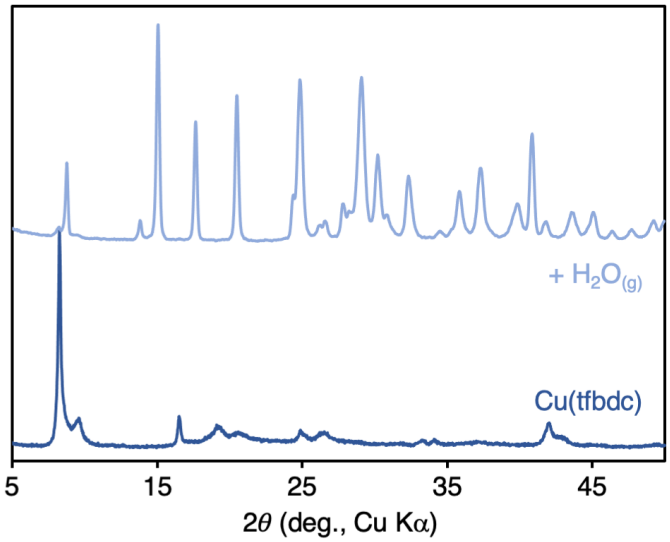

Supplementary Figure 24. Comparison of powder x-ray diffraction patterns collected for microcrystalline Cu(tfbdc) before (dark blue) and after (light blue) exposure to 100% relative humidity at room temperature. Of the materials studied in this work, only Cu(tfbdc) undergoes a phase change upon exposure to gaseous water under these conditions.

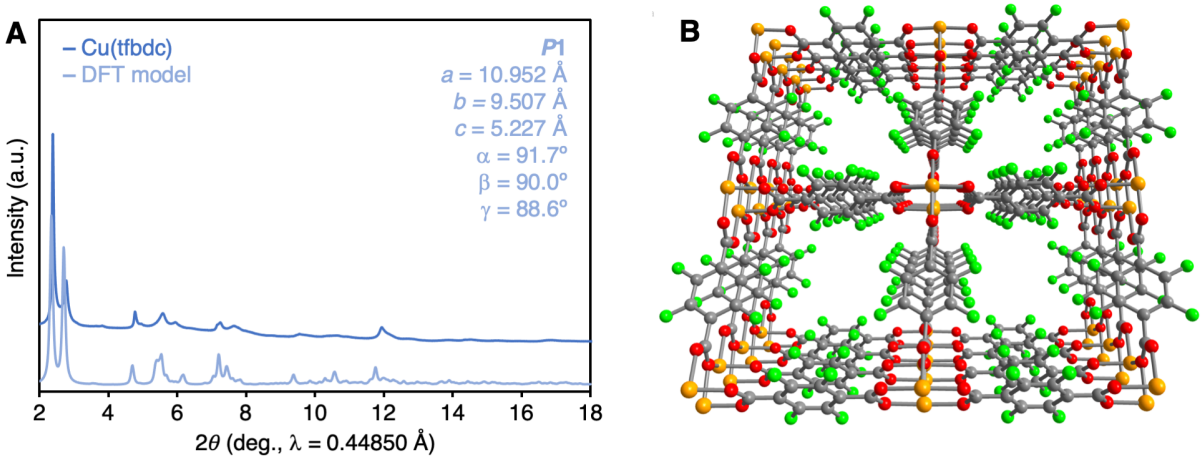

Supplementary Figure 25. (**A**) Synchrotron powder x-ray diffraction pattern of activated Cu(tfbdc) (dark blue), compared to the predicted powder pattern of its DFT model (light blue). (**B**) DFT structural model of Cu(tfbdc). Orange, green, red, and gray spheres represent Cu, F, O, and C atoms, respectively; H atoms have been omitted for clarity. The coordinates of this DFT model are reported in Supplementary Table 4.

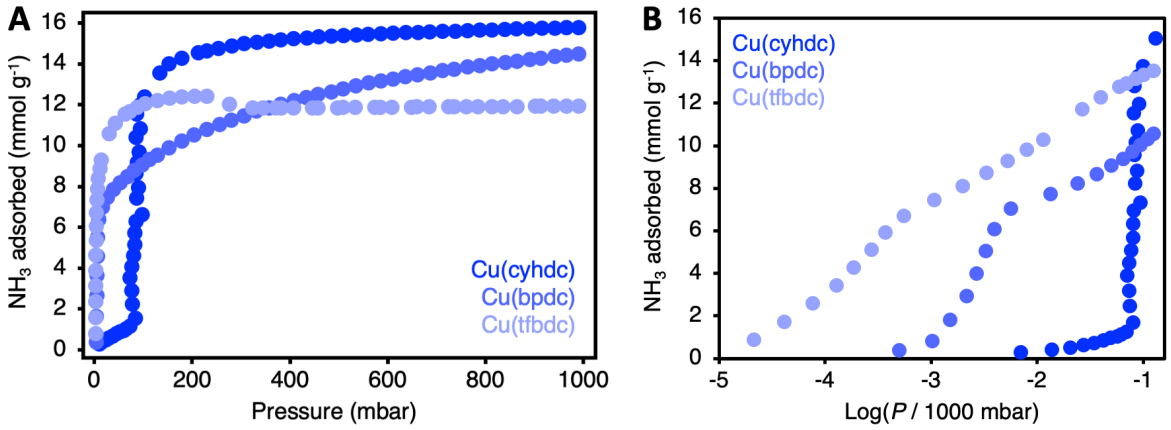

Supplementary Figure 26. Ammonia adsorption isotherms collected at 298 K for Cu(cyhdc), Cu(bpdc), and Cu(tfbdc) plotted with linear (A) and logarithmic (B) pressure scales.

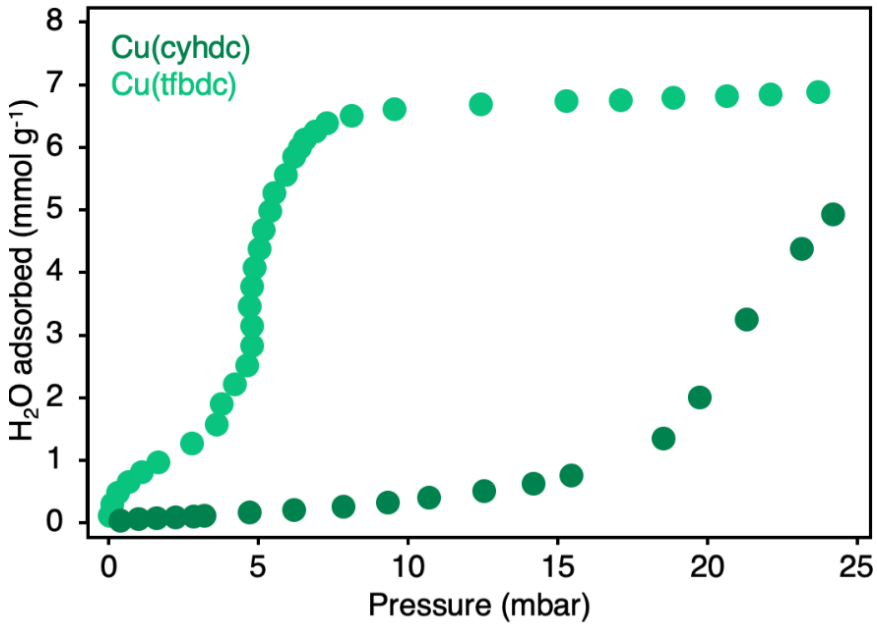

Supplementary Figure 27. Water vapor adsorption isotherms (P_0 = 31.7 mbar) collected at 298 K for Cu(cyhdc) (dark green) and Cu(tfbdc) (light green). Water uptake in Cu(tfbdc) results in a cooperative phase change based on the change in the powder x-ray diffraction pattern that results following exposure to water (see Supplementary Fig. 24). In contrast, the increase in H_2O uptake adsorption for Cu(cyhdc) above 20 mbar is attributed to condensation via pore filling (see Supplementary Fig. 37).

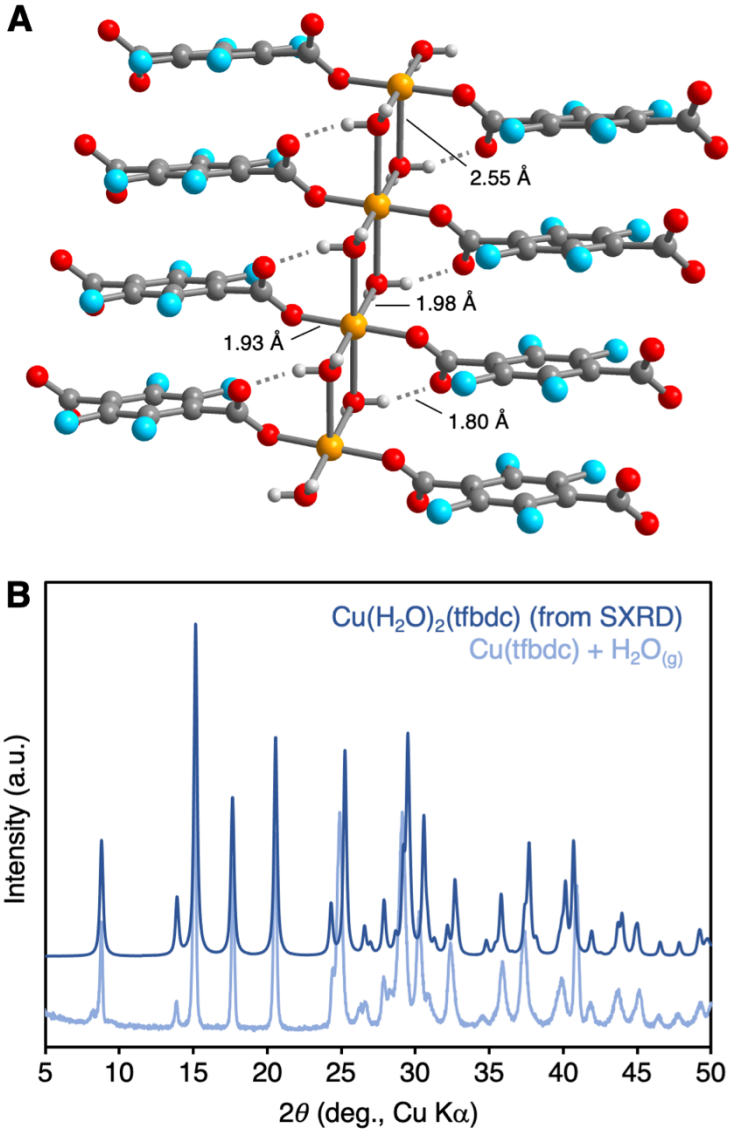

Supplementary Figure 28. (**A**) Portion of the polymeric structure of $Cu(H_2O)_2(tfbdc)$ obtained from x-ray diffraction analysis of single crystals prepared as described in the Methods section. Neighboring polymer chains associate through hydrogen bonding and bridging water molecules. Select bond lengths are indicated; see Supplementary Table 1 for crystallographic data. (**B**) Comparison of the powder x-ray diffraction pattern predicted from the single-crystal x-ray diffraction structure of $Cu(H_2O)_2(tfbdc)$ (dark blue) to the powder x-ray diffraction pattern obtained for a sample of Cu(tfbdc) dosed with air saturated with water vapor (31.7 mbar at 298 K) (light blue).

10. Conversion of $Cu(NH_3)_4(cyhdc)$ into $Cu(NH_3)_2(H_2O)(cyhdc)$ in humid air

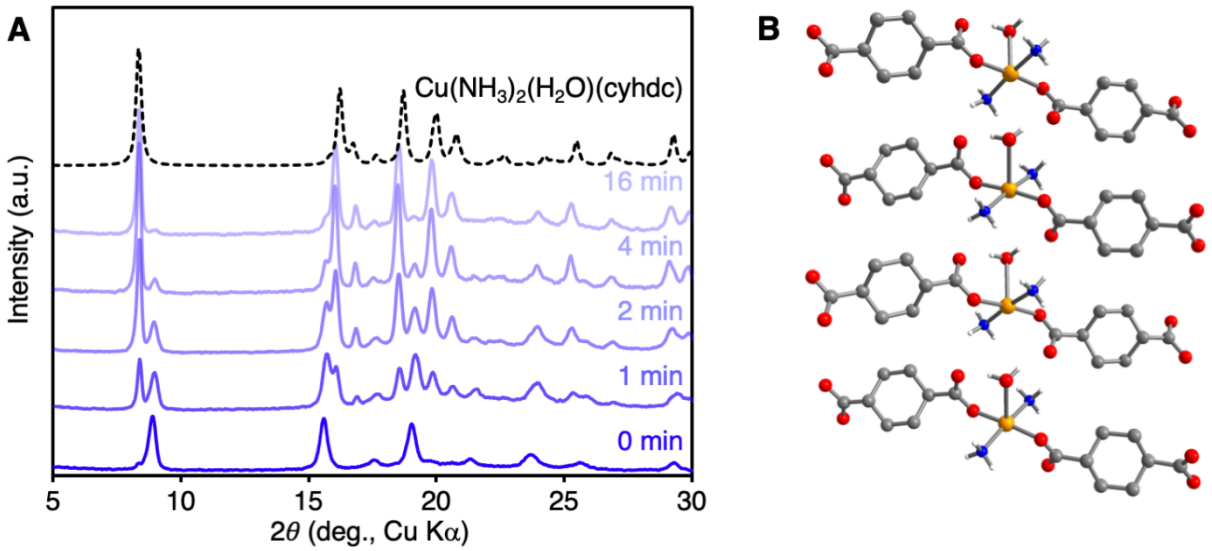

Supplementary Figure 29. (**A**) Powder x-ray diffraction patterns from samples of $Cu(NH_3)_4(cyhdc)$ exposed to ambient atmosphere on a flat surface for various contact times and then sealed inside glass capillaries for analysis. A new crystalline phase appears within one minute, and the conversion of $Cu(NH_3)_4(cyhdc)$ to this new phase is essentially complete after 16 minutes. The powder pattern after 16 minutes of exposure matches the predicted powder pattern of $Cu(NH_3)_2(H_2O)$ (top trace) generated from the single crystal structure of this material, a portion of which is shown in panel (**B**). Orange, red, blue, gray, and white spheres represent Cu, O, N, C, and H atoms; hydrogen atoms are omitted from the $cyhdc^{2-}$ ligand for clarity.

11. Preliminary analysis of the kinetics of NH_3 adsorption in Cu(cyhdc)

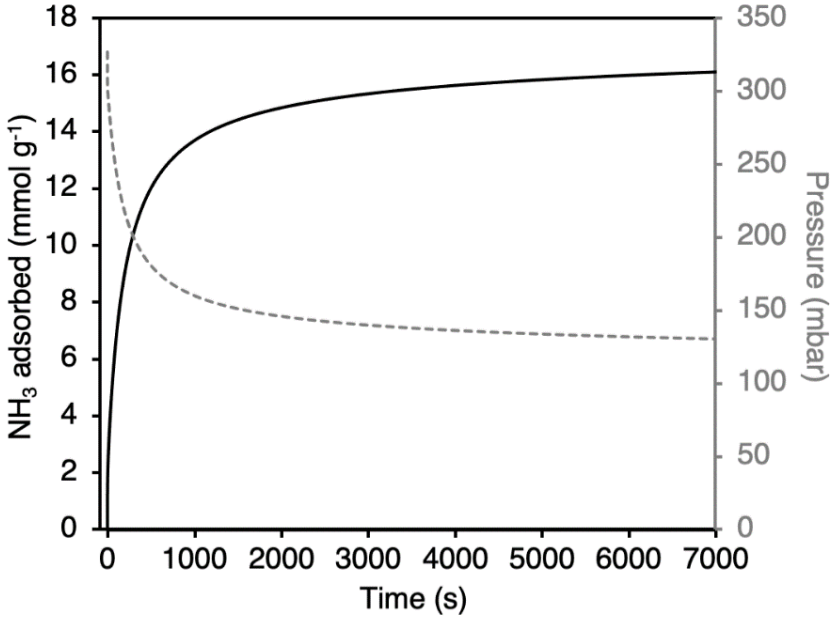

Supplementary Figure 30. Ammonia adsorbed by Cu(cyhdc) over time at 298 K under static conditions as described in the Methods section (black trace). The corresponding pressure trace is shown as a dashed gray line for comparison. Note that adsorption is rapid ($t_{1/2}$ < 150 s) even with an initial ammonia pressure of 326 mbar, which is ~250 mbar above the step pressure. From these data, we can extrapolate a $t_{1/2}$ < 40 s for P_0 = 1 bar (920 mbar above the step pressure).

12. *Ex situ* analysis of Cu(cyhdc) following NH_3 exposure at elevated temperature

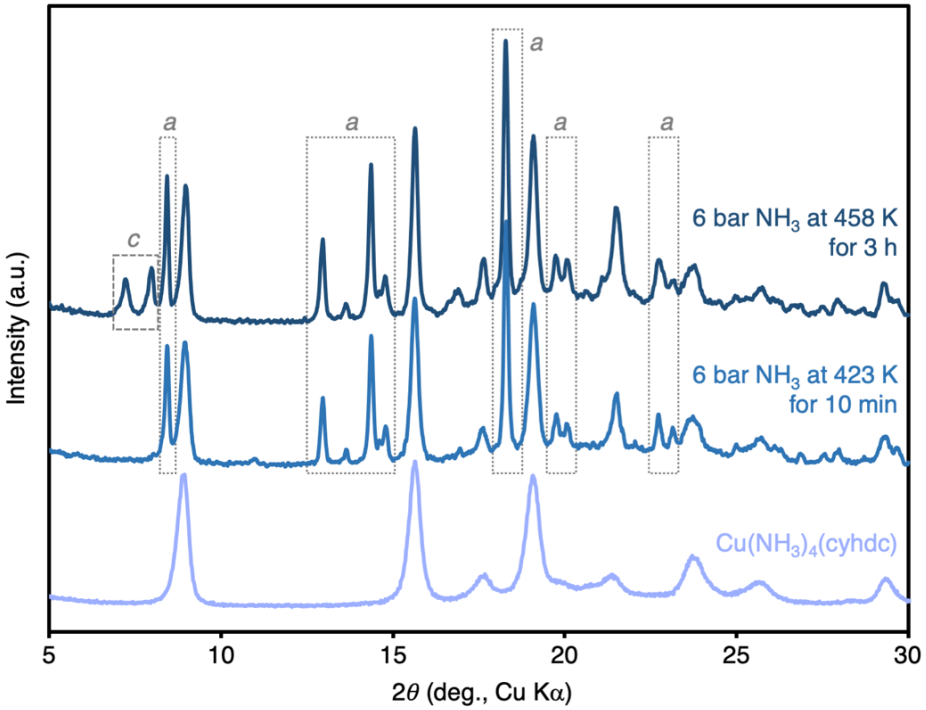

Supplementary Figure 31. Comparison of *ex situ* powder x-ray diffraction patterns for pristine $Cu(NH_3)_4$(cyhdc) (bottom trace), a sample of Cu(cyhdc) dosed with 6 bar of NH_3 at 423 K for 10 min and then cooled to room temperature and depressurized to atmospheric pressure (middle trace), and a sample of Cu(cyhdc) dosed with 6 bar of ammonia at 458 K for 3 h and then cooled to room temperature and depressurized (top trace). Reflections due to components *b* and *c* are labeled.

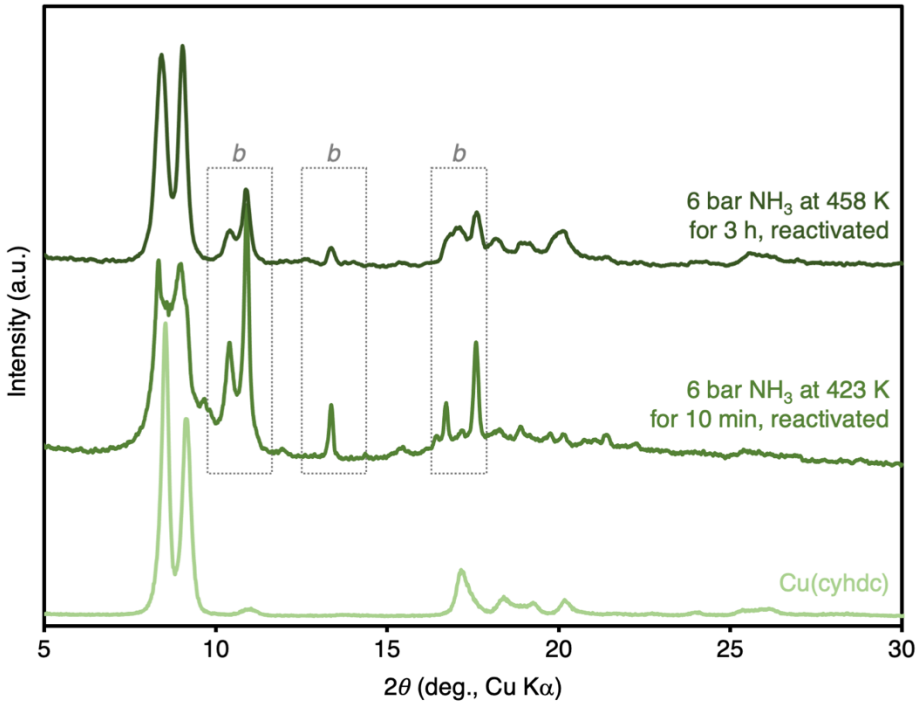

Supplementary Figure 32. Comparison of *ex situ* powder x-ray diffraction patterns obtained for samples of Cu(cyhdc) dosed with NH_3 under the indicated conditions and subsequently re-activated with heating and dynamic vacuum (see Methods for details). The diffraction pattern for pristine Cu(cyhdc) is shown for comparison. Reflections due to component *a* are labeled.

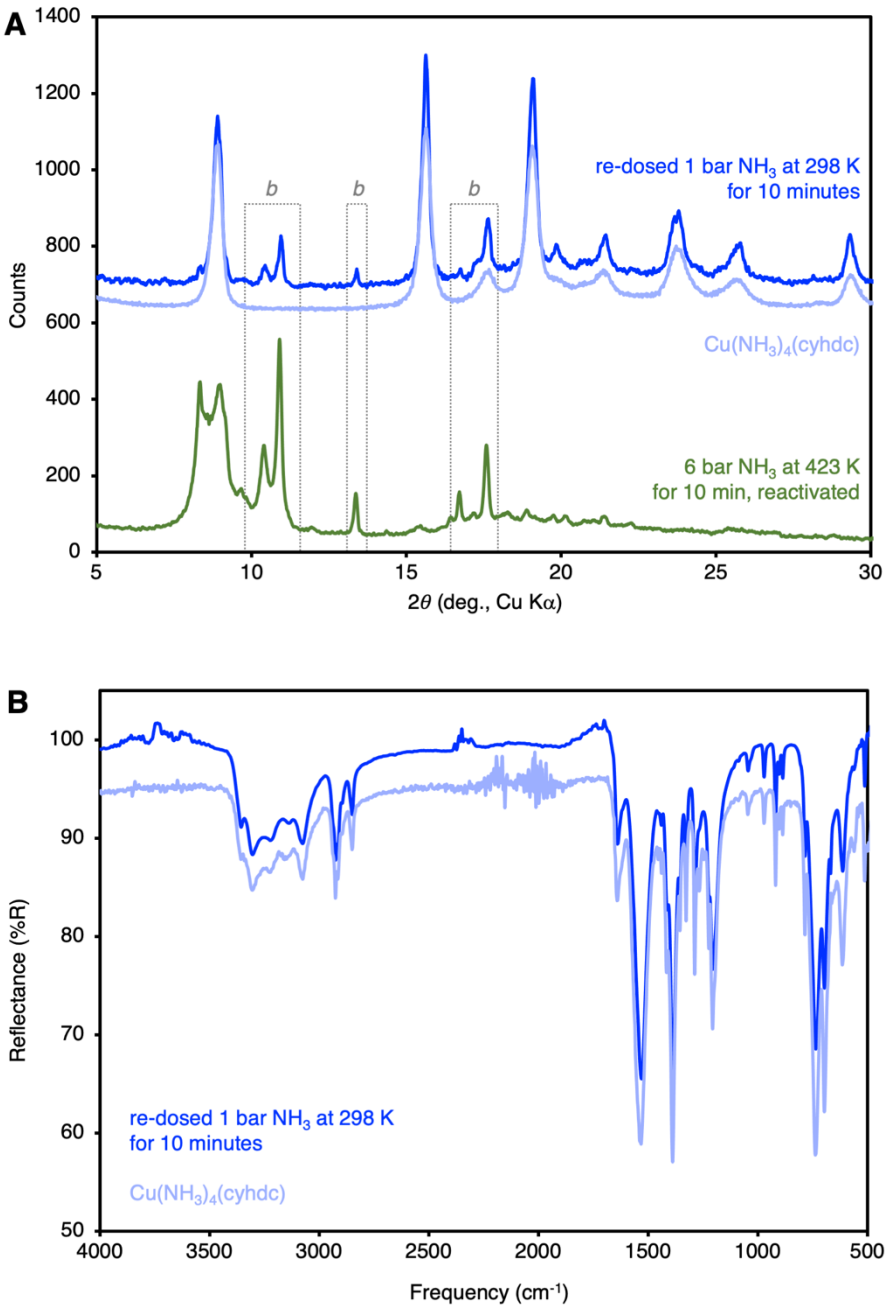

Supplementary Figure 33. (**A**) Comparison of *ex situ* powder x-ray diffraction patterns collected for a sample of Cu(cyhdc) dosed with 6 bar NH_3 at 423 K and subsequently re-activated with heating (165 °C) under dynamic vacuum before (green trace) and after (dark blue trace) re-dosing with 1 bar NH_3 at 298 K for 10 min. Reflections due to component *a* are labeled. Data were collected from sealed capillaries packed to the same height (10 mm) with powder, meaning these patterns can be interpreted semi-quantitatively. The powder x-ray diffraction pattern for $Cu(NH_3)_4$(cyhdc) is shown in pale blue for comparison. (**B**) Comparison of the attenuated total reflectance Fourier transform infrared spectrum of pristine $Cu(NH_3)_4$(cyhdc) with that collected for the same re-dosed sample shown in panel **A** (dark blue).

13. Ammonia adsorption in Cu(cyhdc) from aqueous ammonia vapor

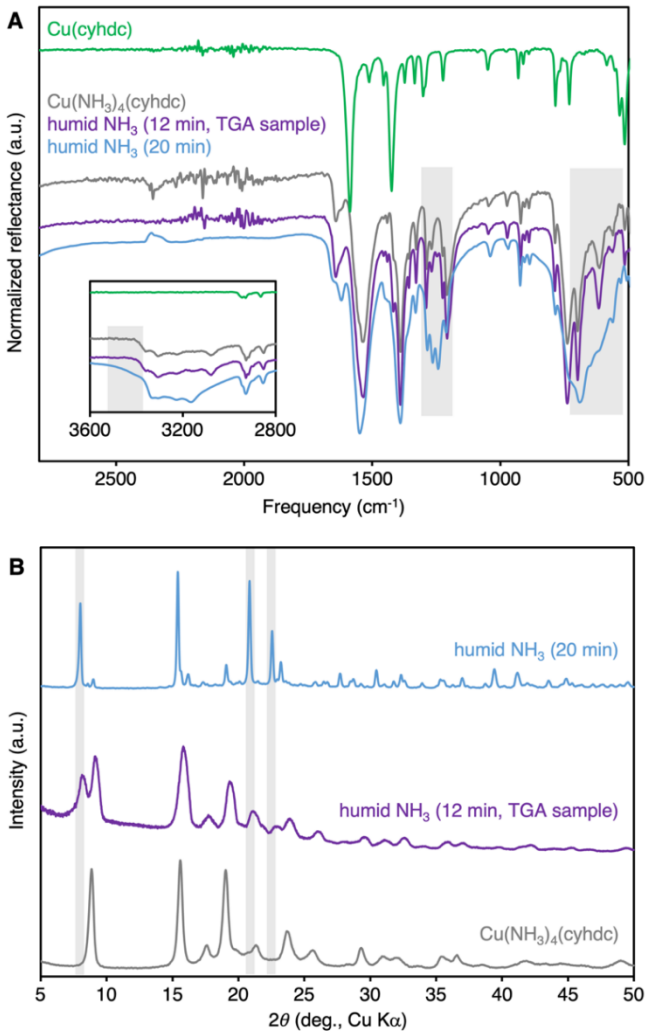

Supplementary Figure 34. Evaluation of water co-adsorption during exposure of Cu(cyhdc) to humid NH_3. (**A**) Comparison of attenuated total reflectance Fourier-transform infrared spectra of Cu(cyhdc) (green trace), $Cu(NH_3)_4$(cyhdc) (gray trace), Cu(cyhdc) dosed with humid ammonia according to the protocol used for TGA cycling (purple trace; 12 min exposure, see the Methods Section and Supplementary Fig. 36), and Cu(cyhdc) after 20 min exposure to humid NH_3 (blue trace, see Methods). Exposure to humid NH_3 for 20 min clearly results in water co-adsorption (blue trace), and distinctive features are highlighted with grey bars at 600 cm^{-1} (broad), 1250 cm^{-1}, and in the inset showing the N-H/O-H stretching region (see shoulder at ~3450 cm^{-1}). (**B**) Powder x-ray diffraction patterns for the corresponding samples in **A**. After exposure to humid NH_3 for 20 min, a new crystalline phase clearly forms (blue trace). Three highlighted reflections from the latter phase can be identified as weaker reflections in the diffraction pattern for a sample of Cu(cyhdc) exposed to humid NH_3 for 12 min (using the TGA sample preparation protocol as described in the Methods, purple trace). However, infrared spectroscopy data for the sample exposed to humid ammonia for 12 min indicate water co-adsorption is minimal under these conditions (panel **A**).

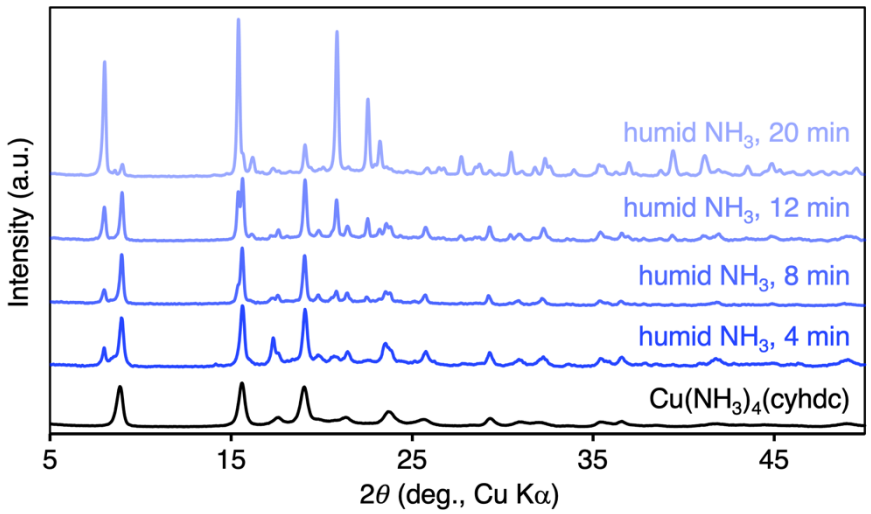

Supplementary Figure 35. Comparison of powder x-ray diffraction pattern collected for a sample of $Cu(NH_3)_4$(cyhdc) prepared by exposing Cu(cyhdc) to dry gaseous ammonia for 30 min (as described in the Methods) to diffraction patterns obtained for samples of Cu(cyhdc) exposed to humid ammonia for various contact times (see Methods for details). After just 4 min, an unidentified phase is visible along with dominant reflections for $Cu(NH_3)_4$(cyhdc). Conversion of $Cu(NH_3)_4$(cyhdc) to this unidentified phase, which presumably contains co-adsorbed H_2O, is nearly complete after 20 min of exposure to humid NH_3 (top trace).

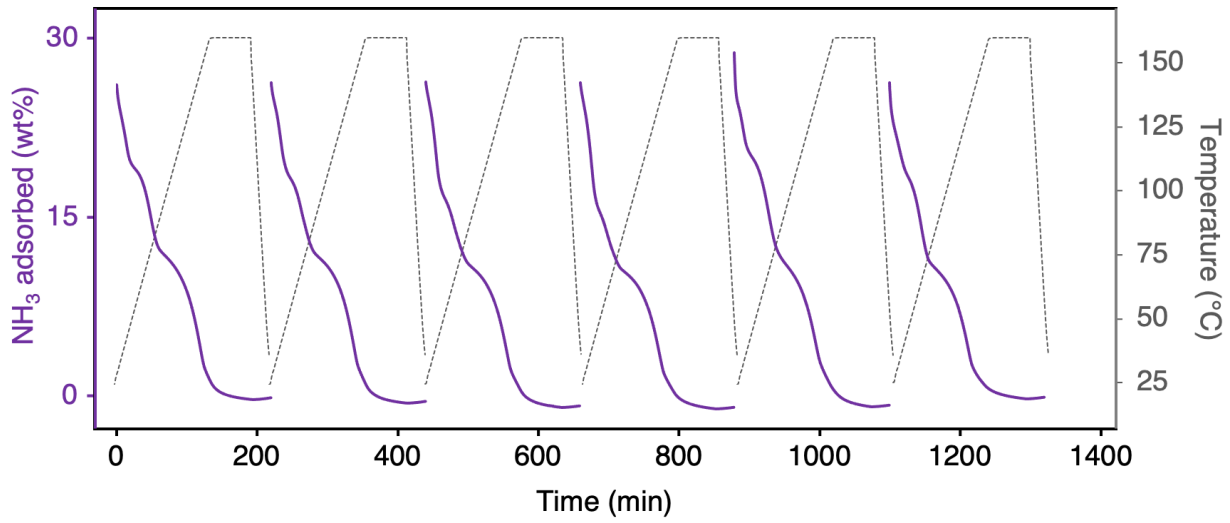

Supplementary Figure 36. Thermogravimetric analysis of NH_3 desorption from $Cu(NH_3)_4$(cyhdc) prepared using humid NH_3 (see Methods and Supplementary Fig. 34) over the course of six cycles. For each cycle, the material was heated from 25 to 160 °C (ramp rate of 1 °C/min), held for 60 min at 160 °C, and then cooled to 25 °C. The sample was subsequently dosed with humid ammonia at 25 °C for 12 min before another desorption cycle.

14. Powder x-ray diffraction analysis of H_2O adsorption by Cu(cyhdc)

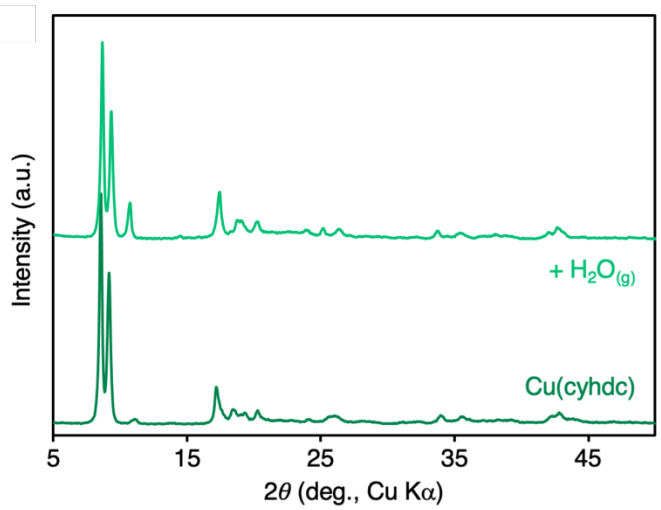

Supplementary Figure 37. Comparison of powder x-ray diffraction patterns collected for microcrystalline Cu(cyhdc) before (dark green) and after (light green) exposure to 100% relative humidity (P_0 = 31.7 mbar) at room temperature.

15. Crystallographic data for copper polymers

Table S1. Crystallographic data

	$Cu(H_2O)_2$(tfbdc)	$Cu(NH_3)_2$(cyhdc)	$Cu(NH_3)_4$(cyhdc)	$Cu(NH_3)_2(H_2O)$(cyhdc)
Formula	$C_8H_4CuF_4O_6$	$C_8H_{16}CuN_2O_4$	$C_8H_{22}CuN_4O_4$	$C_8H_{18}CuN_2O_5$
Temperature (K)	100(2)	100(2)	100(2)	100(2)
Crystal System	Triclinic	Triclinic	Triclinic	Monoclinic
Space Group	$P\bar{1}$	$P\bar{1}$	$P\bar{1}$	$P2_1/c$
a, *b*, *c* (Å)	3.52640(10), 6.4631(3), 10.2064(9)	9.2014(3), 10.1029(4), 11.9356(4)	5.1595(3), 6.4679(4), 9.7393(6)	21.7092(2), 4.86270(10), 11.20010(10)
α, β, γ (°)	99.692(6), 91.108(5), 90.983(3)	95.689(3), 105.608(3), 96.279(3)	82.110(5), 86.794(5), 80.870(5)	90, 102.9150(10), 90
V (Å^3)	229.21(2)	1052.60(7)	317.66(3)	1152.43(3)
Z	1	4	1	4
Radiation, λ (Å)	Cu Kα, 1.54184	Cu Kα, 1.54184	Cu Kα, 1.54184	Cu Kα, 1.54184
2Θ Range for Data Collection (°)	4.396 to 68.266	3.881 to 68.249	4.586 to 73.327	4.179 to 78.787
Completeness to 2Θ	94.2% (2Θ = 67.684°)	99.6% (2Θ = 67.684°)	99.3% (2Θ = 67.684°)	100% (2Θ = 67.684°)
Data / Restraints / Parameters	2288 / 0 / 90	3841 / 0 / 278	1216 / 0 / 81	2421 / 0 / 150
Goodness of Fit on F^2	1.090	1.067	1.064	1.147
R_1[a], wR_2[b] ($I>2\sigma(I)$)	0.0421, 0.1151	0.0449, 0.1173	0.0334, 0.0871	0.0334, 0.0900
R_1[a], $wR2$[b] (all data)	0.0458, 0.1171	0.0623, 0.1274	0.0350, 0.0882	0.0345, 0.0906
Largest Diff. Peak and Hole (e Å^{-3})	1.830 and –0.462	0.953 and –0.800	0.494 and –0.386	0.439 and −0.589

[a] $R_1 = \sum||F_o| - |F_c||/\sum|F_o|$. [b] $wR_2 = \{\sum[w(F_o^2 - F_c^2)^2]/\sum[w(F_o^2)^2]\}^{1/2}$.

16. Coordinates for DFT models

Supplementary Table 2. *x*, *y*, *z* coordinates of $Cu(NH_3)_4$(cyhdc) DFT model.

H	2.59598	2.89764	1.31581
H	0.84879	1.05160	1.32536
O	3.03404	5.66244	-0.57826
O	1.31520	5.81055	0.84440
C	1.64823	3.74177	-0.33575
C	2.01198	5.18129	0.01050
C	0.22009	3.35107	0.03380
H	-0.41689	3.93910	-0.44477
H	0.08406	3.47852	1.00601
C	2.64985	2.79128	0.33301
H	3.56800	3.03160	0.05011
H	-1.96700	-1.07485	-1.54616
O	-0.44064	-0.97611	0.57824
O	1.27820	-1.12423	-0.84442
N	-0.15773	-3.62881	-1.17807
H	0.45522	-2.95950	-1.24423
H	0.23535	-4.36536	-0.81607
H	-0.47676	-3.83099	-2.00588
N	-0.96843	-4.18337	1.55007
H	-1.12893	-3.76065	2.33964
H	-0.07245	-4.30788	1.44936
C	0.94528	0.94458	0.33581
C	0.58152	-0.49488	-0.01057
C	2.37331	1.33525	-0.03382
H	3.01041	0.74734	0.44478
H	2.50934	1.20780	-1.00603
C	-0.05645	1.89504	-0.33303
H	-0.97450	1.65471	-0.05014
H	1.74463	3.63476	-1.32529
H	-0.00258	1.78877	-1.31587
Cu	-1.67808	-3.03236	-0.00002
N	-3.19851	-2.43585	1.17814
H	-3.81147	-3.10521	1.24421
H	-3.59158	-1.69930	0.81614
H	-2.87949	-2.23372	2.00586
N	-2.38781	-1.88130	-1.55000
H	-2.22722	-2.30407	-2.33967
H	-3.28370	-1.75683	-1.44939
H	-1.38925	-4.98986	1.54615
Translation vector 1	6.46784	0.00000	0.00000
Translation vector 2	5.94965	10.75103	0.00000
Translation vector 3	0.81870	2.25414	4.56827

Supplementary Table 3. *x*, *y*, *z* coordinates of Cu(bpdc) DFT model.

H	-0.03120	-0.39000	5.65810
C	-0.54850	-1.18550	6.19820
H	-2.48680	-0.37400	5.68470
C	-1.94290	-1.16670	6.20260
C	-0.11840	3.27480	6.86970
O	-4.73520	-1.13970	6.34510
C	-2.97150	3.30200	6.87290
C	-4.46540	3.31470	6.87410
C	-2.46230	1.23450	-6.21350
C	-3.85650	1.24160	-6.21650
H	-1.95950	0.42610	-5.67940
O	-6.64920	1.26640	-6.34830
H	-4.41520	0.45410	-5.70640
Cu	6.64970	1.08700	-6.29300
O	-6.63930	-2.21350	4.66300
C	-7.01480	1.98270	4.63790
H	-5.73540	-2.54290	2.29420
O	-6.99620	1.21950	5.67350
C	-6.59850	1.99740	2.16150
C	-7.15090	1.36150	3.28890
C	-6.76320	1.45190	0.88990
H	-6.29880	1.96940	0.04840
C	7.37330	0.17750	3.10640
H	6.93350	-0.32680	3.96830
C	-7.51930	0.27230	0.67970
C	7.18080	-0.34200	1.82570
H	6.58340	-1.25080	1.73310
H	-0.00490	0.41710	-5.66590
C	0.51240	1.20960	-6.21050
H	2.45050	0.39930	-5.69490
C	1.90670	1.19000	-6.21590
C	0.08230	-3.25360	-6.88630
O	4.69820	1.15840	-6.36300
C	2.93550	-3.28190	-6.89080
C	4.42940	-3.29620	-6.89300
C	2.42620	-1.21640	6.19240
C	3.82040	-1.22380	6.19510
H	1.92340	-0.41060	5.65430
O	6.61410	-1.24940	6.32720
H	4.37910	-0.43820	5.68210
Cu	-6.68590	-1.07160	6.27540
O	6.60790	2.22210	-4.68030
C	6.98820	-1.97400	-4.65070
H	5.80610	2.49300	-2.29580

O	6.96160	-1.20790	-5.68370
C	6.63920	-2.02980	-2.16540
C	7.14000	-1.36220	-3.29890
C	6.82150	-1.49680	-0.89100
H	6.41120	-2.04920	-0.04370
C	-7.41880	-0.15720	-3.11920
H	-7.01600	0.37130	-3.98420
C	7.53330	-0.28920	-0.68580
C	-7.21870	0.35800	-1.83780
H	-6.66510	1.29450	-1.75060

Translation vector 1	15.25705	0.00000	0.00000
Translation vector 2	-0.30286	5.46855	0.00000
Translation vector 3	1.59334	1.04511	13.75458

Supplementary Table 4. *x*, *y*, *z* coordinates of Cu(tfbdc) DFT model.

Cu	5.35350	-4.05120	-1.51140
O	-3.65140	-4.11630	-1.62100
O	5.36840	-2.34560	-2.54130
O	-3.41890	4.09940	1.63140
C	-3.07020	-4.84070	2.61610
O	5.35850	-3.59990	0.69610
C	5.37960	-2.54820	1.42220
C	-1.56800	-4.83990	2.61340
F	-1.41340	-3.21480	-0.70940
C	-0.82390	-3.95120	-1.66350
C	5.42330	-1.23230	0.69060
C	-0.58900	3.93860	1.66240
F	-1.18070	3.20240	0.70990
C	-4.30380	-0.61250	0.42240
F	-3.15710	-1.18970	0.83020
F	3.05380	-1.18060	0.53130
C	4.24440	-0.60900	0.26970
Cu	-5.36630	4.03960	1.50800
O	3.63850	4.10380	1.61820
O	-5.37970	2.33390	2.53780
O	3.40600	-4.11010	-1.63520
C	3.05720	4.82920	-2.61950
O	-5.37300	3.58820	-0.69960
C	-5.39240	2.53650	-1.42570
C	1.55510	4.82850	-2.61700
F	1.40040	3.20360	0.70570
C	0.81090	3.93980	1.65990
C	-5.43620	1.22060	-0.69410
C	0.57610	-3.94980	-1.66600
F	1.16780	-3.21360	-0.71360
C	4.29100	0.60080	-0.42590
F	3.14430	1.17800	-0.83370
F	-3.06660	1.16890	-0.53500
C	-4.25720	0.59730	-0.27330
Translation vector 1	10.95186	0.00000	0.00000
Translation vector 2	0.23254	9.50375	0.00000
Translation vector 3	0.00427	-0.16083	5.22449